

Gridtoplate currentvoltage characteristics of a corona triode

O. N. Oliveira and G. F. Leal Ferreira

Citation: Rev. Sci. Instrum. 56, 1957 (1985); doi: 10.1063/1.1138452

View online: http://dx.doi.org/10.1063/1.1138452

View Table of Contents: http://rsi.aip.org/resource/1/RSINAK/v56/i10

Published by the American Institute of Physics.

Related Articles

Bidirectional operation of vertical organic triodes J. Appl. Phys. 111, 044507 (2012)

Modification of anisotropic plasma diffusion via auxiliary electrons emitted by a carbon nanotubes-based electron qun in an electron cyclotron resonance ion source

Rev. Sci. Instrum. 83, 02A343 (2012)

The design of an electron gun switchable between immersed and Brillouin flow

Rev. Sci. Instrum. 83, 02A506 (2012)

Numerical study of an 8mm third-harmonic peniotron with a gradual reversal of the magnetic field Phys. Plasmas 19, 023101 (2012)

Thermal-structural analysis of electron gun with control grid

Rev. Sci. Instrum. 83, 024701 (2012)

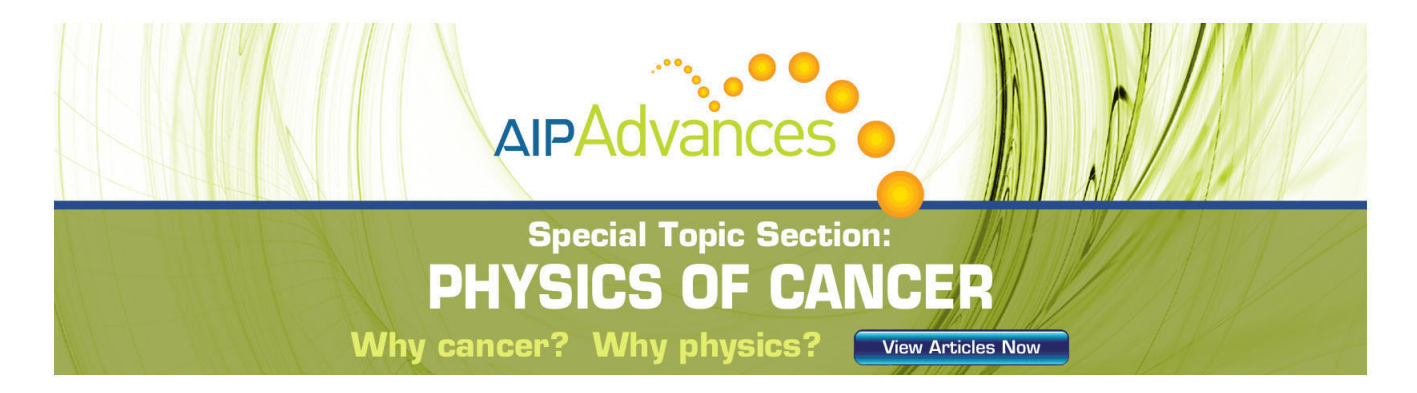
Additional information on Rev. Sci. Instrum.

Journal Homepage: http://rsi.aip.org

Journal Information: http://rsi.aip.org/about/about_the_journal Top downloads: http://rsi.aip.org/features/most_downloaded

Information for Authors: http://rsi.aip.org/authors

ADVERTISEMENT



Grid-to-plate current-voltage characteristics of a corona triode

O. N. Oliveira, Jr. and G. F. Leal Ferreira

Institute of Physics and Chemistry of São Carlos, University of São Paulo, C.P. 369-13.560-São Carlos-S.P.-Brazil

(Received 5 March 1985; accepted for publication 27 June 1985)

Measurements of the grid-to-plate current-voltage characteristics of the corona triode are reported. A space-charge-limited current (SCLC) characteristic is observed to hold for low values of the plate current I_P , provided that the grid voltage V_g is corrected for a counter potential V_r . The analysis of experimental results indicates that V_r is due both to penetration of field lines through the grid and to the corona wind. However, departure from SCLC regime is observed at higher plate currents, when the ion supply from the corona current becomes insufficient to afford it. A simplified theory is developed in order to explain the results. In the calculation, a layer of recombination centers is substituted for the grid. The model fits the whole characteristics and leads to reasonable value of the parameters defined by the model.

INTRODUCTION

The corona triode with constant current^{1,2} has been extensively used by the authors in the study of charge transport in thin polymer films. It consists of (1) a metal point where a high potential is applied to generate ions by a corona discharge, (2) a grid biased at a certain voltage, usually far below that of the point, and (3) the grounded plate, below the grid, where the sample to be charged rests (see Fig. 1).

The following symbols will be used henceforth: I_c -corona current; V_c -needle potential; V_g -grid potential; I_p -plate current; V_r -counter potential; $V_{gc} = V_g + V_r$ -corrected grid potential.

All the quantities will be taken as positive, irrespective of the polarity. The potentials are taken relative to the plate.

In this work, no sample was used and the plate current, that is, that crossing the grid, was studied as a function of the grid potential for various corona currents of both polarities. We have observed that for zero grid potential the plate current I_p is not zero and a certain counter voltage V_r has to be applied in order to cancel it. If the grid potential V_g is corrected for this value, the characteristics I_p vs $(V_g + V_r)$ may directly be interpreted as being space-charge limited, as should be expected. However, departure from the space-charge characteristic behavior is observed for higher plate currents.

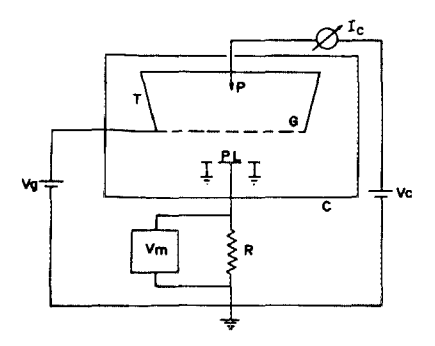


FIG. 1. Experimental setup shown schematically, P-metal point. G-grid, T-thin-walled metal cone, PL-plate, I_c -corona current ammeter, V_c -needle voltage supply, V_g -grid voltage supply, R-10-M Ω resistor, V_m -voltmeter, C-external case.

The counter voltage V, was measured as a function of the corona current and the results seem to indicate that besides the penetration of field lines through the grid, another cause must be invoked to explain them. We have tentatively assumed that a corona wind of mean speed 20 cm/s passes through the grid, but no attempt was made here to measure it directly. See however the results by Goldman $et\ al.^3$ on this subject.

Section I shows the experimental setup and Sec. II the most significant experimental results. In Sec. III a theory is developed to explain in a simplified way the main results, and Sec. IV discusses the attained fair agreement.

I. EXPERIMENTAL

The experimental setup used in our measurements is the corona triode recently developed for charging polymer foils with a constant current. The essential features of the apparatus are shown in Fig. 1. Corona voltage V_c is originated from a Spellman high-voltage Supply (0–30 kV), while the grid is biased by a Fluke High Voltage supply, model 410B (0–10 kV). The corona current I_c is measured by a Kioritsu Microamperes dc (0–50 μ A) ammeter and the plate current I_p is obtained by the voltage drop across a resistance of 10 M Ω in series with the air gap. This voltage drop is measured by means of a Keithley Electrometer type 602.

The corona point P is an inexpensive sewing needle of nickel-plated steel. Concentrically it is shielded by a thin-walled metal cone in order to avoid current flux toward the external case. For small point-to-grid distances d used in this work, around 2.2 cm, only a few per cent of the corona current (higher for negative than for positive polarity) reaches the cone. The plate consists of a central electrode usually of 5 cm² surrounded by a guard ring (external radius 1.9 cm). The grid-to-plate distance l varied from 0.4 to 2.4 cm. However, in one of the experiments it was increased to 7.0 cm, and in this case, the central electrode was decreased to 3.1 cm² in order to ensure uniformity on the measured region.

The grid is a composite one, made of two close layers looking like a lens, the convex face standing downward. Such a shape introduces an uncertainty of about 1 mm in the

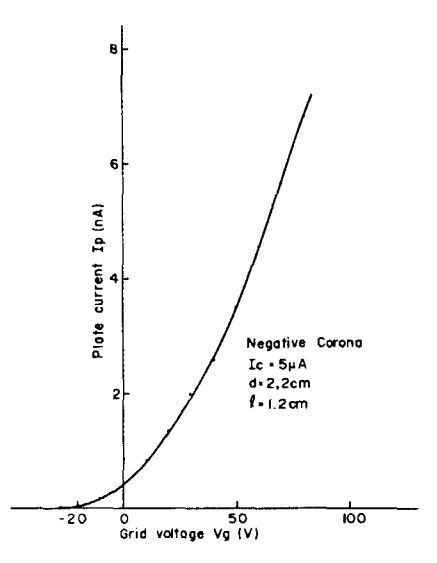


FIG. 2. Quadratic behavior of $I_p X V_g$ characteristics for negative corona with fixed geometry. The counter potential V_r is here 27 V (I_p plate current, V_o grid voltage).

grid-to-plate distance, but this shortcoming is amply compensated for by a greater uniformity of charge deposition.^{2,4} The grid area is 78.5 cm².

II. RESULTS

1958

Figure 2 shows I_p vs V_g parabolic characteristics, obtained for a constant negative corona current $I_c = 5 \,\mu\text{A}$, $d = 2.2 \,\text{cm}$ and $l = 1.2 \,\text{cm}$. It is seen that for $V_g = 0$, I_p is not zero, as anticipated in the Introduction. On the other hand $I_p = 0$ for $V_g = -V_r = -27 \,\text{V}$. If we add V_r to V_g , obtaining V_{gc} , and plot log V_{gc} vs log I_p we get Fig. 3. Here results are shown for fixed geometry ($d = 2.2 \,\text{cm}$, $l = 1.2 \,\text{cm}$); two positive corona currents ($I_c = 5 \,\text{and} \, 2 \,\mu\text{A}$) and one

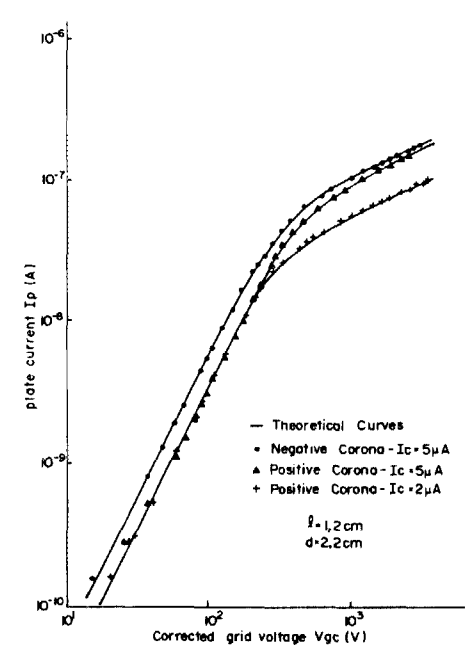


FIG. 3. $\log I_p X \log V_{gc}$ theoretical curves derived from Eq. (11) fitting the experimental points for positive $(I_c = 2 \text{ and } 5 \, \mu \text{A})$ and negative corona $(I_c = 5 \, \mu \text{A})$. $(I_p$, plate current, V_{gc} corrected grid potential).

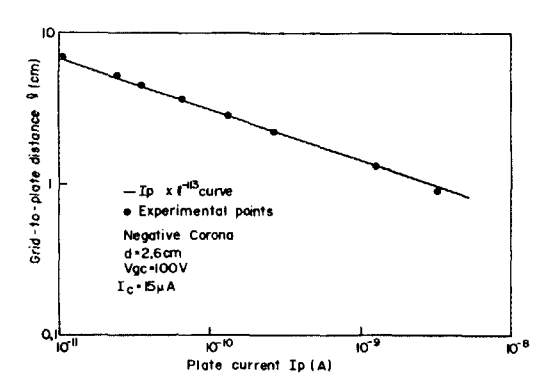


FIG. 4. log-log straight line of the grid-to-plate distance l and the plate current I_p for given negative corona current ($I_c = 15 \,\mu\text{A}$) and constant corrected grid potential ($V_{gc} = 100 \,\text{V}$), showing the dependence $l \propto I_p^{-1/3}$.

negative current $(I_c = 5\mu A)$. The following points should be noted: (1) in all cases, for low V_{gc} , $I_p \propto V_{gc}^2$; (2) for low V_{gc} , the ratio of the currents obtained for both polarities is 1.7; (3) changing I_c does not change the low-voltage behavior of I_p ; (4) for higher V_g , $I_p \propto V_{gc}^{1/\gamma}$, γ being almost the same for both polarities ($\gamma \simeq 2.1$), and practically independent of the corona current; (5) the knee of the log I_p vs log V_{gc} curves starts at lower values of V_{gc} for lower I_c .

The quadratic dependence $I_p \propto V_{gc}^2$ suggests a space-charge-limited current regime (SCLC). In order to check this, plate currents at a constant potential ($V_{gc}=100 \text{ V}$) were measured for various plate distances l, for constant negative $I_c=15~\mu\text{A}$ and d=2.6 cm. In this kind of measurement the smaller central electrode was used in order to ensure, for higher l, planar symmetry in the measured region, as close as possible. The results are shown in Fig. 4, giving $l \propto I_p^{-1/3}$ and then confirming the SCLC regime.

We have also studied the experimentally defined variable V_r as a function of l, for some I_c (for both polarities, 1, 3, and 5 μ A) and fixed d=2.3 cm. The results are shown in Fig. 5, for l varying from 0.4 to 2.4 cm. It is seen that straight

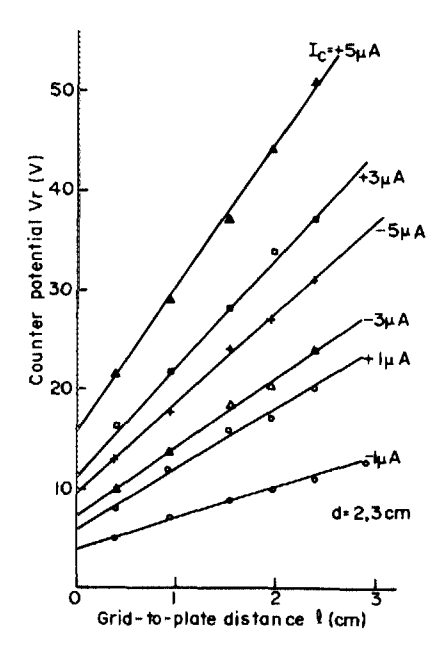


Fig. 5. V, Xl straight lines for several corona currents, both negative and positive corona. V, is the counter potential and l the grid-to-plate distance.

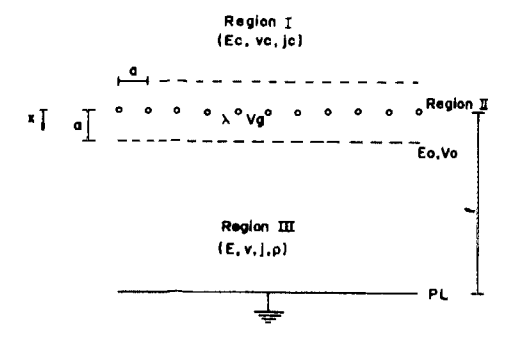


FIG. 6. Schematic model for the theory developed in Sec. IV. Region I, the corona space, ends a distance a from the grid, where the electric field and the density of corona current are E_c and j_c ; V_c is the corona voltage. Region II is the grid region of 2a thickness, the small radius r wires, spaced a, with linear charge λ , and voltage V_g . Region III is the plate space of thickness $l-a\simeq l$, electric field E, current density j, charge density ρ . E_0 and V_0 are the electric field and the voltage just in the beginning of this region. PL represents the plate.

lines well represent the results and both the slope as well as the extrapolated intercepts are higher for positive corona, for the same value of I_c (here d=2.3 cm). For higher values of l, the plate current at $V_g=0$, or less, becomes very small and consequently the measurement of V_r , is too inaccurate. We have observed a less than proportional behavior of V_r , with l, for these high values of l, but we do not know if this result is significant in view of the foregoing assertion.

III. THEORY

A. Fields and potentials

Aiming to interpret the results presented in the previous section, a simplified model will be developed. First, in order to make the problem easier mathematically, an array of parallel fine wires of radius r, equally a spaced, was the substitute for the grid. We assume r < a < l. Fig. 6 shows the grid-plate neighborhood, divided into three regions:

Region I-distance a from the grid marks the end of the corona space. The "mean" electric field is E_c , downwards.

Region II-is the grid region, of width 2a. The linear charge density on the wires is λ and V_g their potential. A coordinate axis x, oriented downward, has its origin in the plane passing through the center of the grid wires.

Region III—the plate region, of thickness $l-a \approx l$, where all the quantities are supposed to depend only on x. The electric field and the potential on the boundary with Region II are E_0 and V_0 .

The following relations may be written from the theory of the grid potential:⁵

$$V_g-V_0=-rac{\lambda}{2\pi\epsilon_0}\lnrac{2\pi r}{a}+rac{\lambda}{\epsilon_0}\,,$$
 and
$$E_0=E_c+rac{\lambda}{a\epsilon_0}\,,$$

where ϵ is the vacuum permittivity.

Contribution from space charge is neglected in Eq. (1), owing to the relatively high ion velocities. From these equations the unknown λ may be eliminated to give:

$$V_0 = V_g + (E_0 - E_c) \frac{a}{2\pi} \ln \frac{2\pi r}{a} + (E_0 - E_c)a$$
 (2)

Now, we assume that the corona wind passes through the grid, communicating a drift mean velocity v_0 to the ions. Therefore, the total velocity of the ions and the current density j are

$$v = v_0 + \mu E \,, \tag{3}$$

$$j = \rho v$$
, (4)

 μ being the mobility and ρ the charge density.

Using the Poisson equation, together with Eqs. (3) and (4) we have

$$\epsilon_0 \frac{dE}{dx} = \frac{\epsilon_0}{\mu} \frac{dv}{dx} = \rho = \frac{j}{v},$$

whose integration in x, from a to x leads to

$$v^2 = v_a^2 + \frac{2\mu j}{\epsilon_0}(x - a), \qquad (5)$$

where v_a is the total velocity at a.

Now, V being the potential and using Eq. (3),

$$\frac{dV}{dx} = -E = \frac{v_0 - v}{\mu} \,.$$

Replacing the value of v given in Eq. (5) and integrating over x from a to l, we get

$$V_0 = -\frac{v_0 l}{\mu} + \frac{\epsilon_0}{3\mu^2 j} \left[\left(v_a^2 + \frac{2j\mu l}{\epsilon_0} \right)^{3/2} - v_a^3 \right],$$

since the potential at a is V_0 .

Substituting the value of V_0 given in Eq. (2) we can cast this in the following way:

$$V_g + \frac{v_0 l}{\mu} + (E_c - E_0) a \left(1 + \frac{1}{2\pi} \ln \frac{a}{2\pi r} \right)$$

$$= \frac{\epsilon_0}{3\mu^2 j} \left[\left(v_a^2 + \frac{2j\mu l}{\epsilon_0} \right)^{3/2} - v_a^{-3} \right]. \tag{6}$$

We find here a expression for V_{\perp}

$$V_r = +\frac{v_0 I}{\mu} + E_c a \left(1 + \frac{1}{2\pi} \ln \frac{a}{2\pi r}\right).$$
 (6a)

In Eq. (6a) we have omitted E_0 in the factor $E_c - E_0$ since for small V_g , that is in SCLC regime, E_0 is at most of the order of v_0/μ and this is much less than E_c , the electric field above the grid. On the other hand, for large V_g , the counter potential becomes unimportant and it does not matter whether E_c or $E_c - E_0$ is kept in Eq. (6). So, we have used a constant V_r , in our calculation. Note that the first term in the above expression depends on the corona wind v_0 and the second on the penetration of field lines through the grid, hereafter called V_f . Thus, V_r is written as

$$V_r = +\frac{v_0 l}{\mu} + V_f, \qquad (7)$$

with

$$V_f \simeq E_c a \left(1 + \frac{1}{2\pi} \ln \frac{a}{2\pi r} \right).$$

We make the assumption that a grid of square mesh, simple or double, leads to an expression essentially the same as Eq. (7).

Hence, we may write, using Eqs. (5) and (6) and the previously defined $V_{gc} = V_g + V_r$,

$$V_{gc} = \frac{\epsilon_0}{3\mu^2 i} \left[\left(v_a^2 + \frac{2j\mu l}{\epsilon_0} \right)^{3/2} - v_a^3 \right]. \tag{8}$$

Two regimes are derived from Eq. (8)

$$V_{gc} \simeq \sqrt{\frac{8 l^3 j}{9 \mu \epsilon_0}} \quad v_a^2 < \frac{2j\mu l}{\epsilon_0},$$
 (8a)

$$V_{gc} \simeq \frac{lv_a}{\mu} \quad v_a^2 > \frac{2j\mu l}{\epsilon_0}$$
 (8b)

In the first case, Eq. (8a), the current j is space-charge limited and thus independent of the ion supply to the grid, and in the second case, Eq. (8b), no space charge is present, the current being uniform through the gap.

B. Relation between the corona current and the plate current

The following calculation attempts to relate the plate current I_p to the corona current I_c . We assume that part of the incoming corona current is directly "absorbed" by the grid. We note that, for V_g that is not too high, the overall charge on the grid is negative (for a positive corona) because $E_c > E_0$ and, therefore, we may suppose that the incoming positive current "recombines" with the negative charge of the grid while passing through it. In the calculation below, the grid will be considered as a negatively charged region of very small thickness h (possibly equal to 2a). Following the model calculation by Hughes⁶ we assume here a bimolecular recombination between positive charge on the corona and negative charge on the grid, of density (very high) $\rho_0 = \lambda / ah$. In the Hughes calculation the "recombination" centers are embedded in an insulator of dielectric permitivity ϵ ; in our case ϵ will be used as a mean dielectric constant of the grid region.

The variation of the current due to the recombination is

$$\frac{dj}{dx} = -\alpha\rho\rho_0,$$

where α is the recombination coefficient.

As said previously the space charge of the moving ions will be neglected. Then, using the Poisson equation

$$\epsilon \frac{dE}{dx} = \rho - \rho_0 \simeq -\rho_0,$$

and combining it with Eqs. (3) and (4) there results

$$\frac{dj}{j} = \frac{\alpha \epsilon}{\mu} \frac{dv}{v} \,.$$

Integrating this over the thickness h, we have

$$j = j_c \left(\frac{v_a}{v_c}\right)^{\alpha \epsilon / \mu} ,$$

where j_c is the corona current density, and v_c the velocity of the ions above the grid, at the end of region I. j/jc may be called the electrical transparency of the grid.⁷ Calling

$$\gamma = \mu/\alpha\epsilon$$
 and $q = v_c/f_c^{\gamma}$, (9)

we write

$$v_a = q j^{\gamma}. {10}$$

Substituting this in Eq. (8), we get

$$V_{gc} = \frac{\epsilon_0}{3\mu^2 j} \left[\left(q^2 j^{2\gamma} + \frac{2j\mu l}{\epsilon_0} \right)^{3/2} - q^3 j^{3\gamma} \right]$$
 (11)

In our case γ is around 2.1. The typical current density value separating the two extreme regimes, as given by Eqs. (8a) and (8b), is $(2\mu l/q^2\epsilon_0)^{1/(2\gamma-1)}$; Child's law holds for current densities much less than this value.

IV. DISCUSSION

We have seen that if the potential is corrected for V_r , the counter potential, the results for lower voltages are easily explained as being due to SCLC regime. The charge reservoir at the injecting electrode—the grid—is afforded by the ions of the corona current. The ratio of the currents for a given voltage in this regime, in Fig. 3 is 1.7 within the accepted values of the ratio of the negative to the positive mobilities in air. The results of Fig. 4 bring additional support to this interpretation. The theory developed in Sec. III provides the approximation in Eq. (11) to explain this low-voltage behavior.

More interesting to discuss is the dependence of V_r , on I for constant corona current (Fig. 5) and the high-voltage behavior of the characteristics I_p vs V_{gc} . Of course, the theory has many shortcomings, perhaps the most important being the assumption of a constant corona wind in the grid-plate space. We expected to detect a deviation from the quadratic behavior at low currents due to the nonuniformity of the wind near the plate but this was not observed: the measured V_r led without any corrections, to very good SCLC straight lines in the log-log plot. Another simplification was the use of planar symmetry when the incoming corona current den-

TABLE I. List of the values of the parameters v_0 (corona wind speed) and V_f (contribution to the potential from field line penetration effect), for several corona currents I_c (and the respective needle potentials V_c), and for both polarities, v_0 and V_f were taken from Fig. 5 using Eq. (7). The mobilities obtained in Fig. 3 are also given.

Positive corona ($\mu = 1.38 \text{ cm}^2/\text{Vs}$)				Negative corona ($\mu = 2.30 \text{ cm}^2/\text{Vs}$)			
<i>I_c</i> (μA)	υ _ο (cm/s)	V_f (V)	<i>V_c</i> (kV)	Ι _c (μΑ)	v ₀ (cm/s)	$V_f = (V)$	<i>V_c</i> (kV)
1	8.0	5.6	4.6	1	6.2	3.8	4.2
3	14.4	11.0	6.4	3	13.8	7.2	5.2
5	19.0	15.4	7.4	5	18.2	9.2	6.0
8	24.3	18.4	8.8	8	22.0	12.0	6.9
10	27.5	21.6	9.4	10	26.6	13.2	7.4

TABLE II. γ and $q_{\rm exp}$ parameters as extracted from the fitting of the curves on Fig. 3 to Eq. (11). $q_{\rm th}$ is an approximate value in order to compare with the experimental one.

Polarity	$I_c \ (\mu A)$	γ	$[s^{-1}(A/cm^2)^{\gamma}]$	$[s^{-1}(A/cm^2)^{\gamma}]$
+	2	2.22	5.0×10 ²⁰	3.0×10^{20}
+	5	2.02	4.0×10^{18}	1.6×10^{18}
	5	2.08	1.6×10^{19}	0.6×10^{19}

sity has a strong dependence⁸ on the radial distance measured from the center of the grid. It is true that the lens shaped double layer grid used in this work certainly helped in this respect, as we could verify working also with simple grids, but we do not know how much. Finally, the idea of approximating the behavior of the grid by a layer of a charge absorber was suggested by the calculation of Ref. 6 whose power law relation just fits the behavior of grids at large currents, as we have verified in many cases in our laboratory.^{2,4} As stressed at the end of this section, planar grids seem to be less adequately described by this theory.

Four parameters spring out of the theory: the wind velocity v_0 , the field penetration contribution to the counter potential V_f , Eq. (7), and q and γ defined in Eq. (9). The first two were obtained from Fig. 5 and shown in Table I, together with the mobilities.

The need for assuming a corona wind comes from Fig. 5 and Eq. (7). If the contribution to V_r came solely from V_f , V_r would not depend on l, the grid to plate distance. But undoubtedly this is not the case. Assumption of a corona wind was the way found to explain the dependence on l. As Table I shows, the wind velocity v_0 is about the same for both polarities (\sim 20 cm/s) and as it should, v_0 increases with the corona current. It is of the order predicted by Loeb⁹ (calculated from the momentum transfer brought by the thermalized ions) and less than that measured by Goldman et al.³ (3 m/s). Keeping in mind that our v_0 represents a mean value this difference may be explained by the following reasons: (1) Our grid is a double one, of thicker wires, offering higher impedance to the air flux. (2) In our set up, the plate certainly laterally deviates the air flow, decreasing its mean normal speed. (3) Finally, our measurements were carried out with higher point-to-grid distance (d = 2, 3 cm), while Goldman et al.3 have used 0.5 mm. Obviously short distances yield higher wind velocity.

The other parameter V_f is a little higher for positive than for negative corona. This is understandable in view of the fact that it depends on the point corona potential and this is higher for positive than for negative polarity for the same corona current (corona currents are larger for negative corona than for positive one).

The other two parameters, q and γ , were obtained from Fig. 3, and the results are shown in Table II. According to

Eq. (9), $\gamma = \mu/\alpha\epsilon$, and it should be independent on the corona currents and voltages. The results for positive polarity point are in this direction. Moreover, we observe that γ for negative is about the same as that for positive, that is $\simeq 2.1$. Indeed, if the recombination coefficient of the grid were purely of the Langevin type, ¹⁰ γ would be the same for both polarities and equal to 1. However, most of the grids^{2,4} lead to a γ of about 2.

We turn now to the parameter q. In Table II, under the head $q_{\rm exp}$, are given the values obtained from Fig. 3. In the next row, we give $q_{\rm th}$ as calculated from Eq. (9), $q=v_c/J_c^{\gamma}$, with the following approximations:

First, neglecting the corona wind in the corona space, $v_c \simeq \mu E_c$; E_c will be taken as $(V_c - V_g)/d$, as suggested in Ref. (8); j_c is put as I_c/A , where A is the grid area. With these assumptions, $q_{\rm th}$ becomes $\mu(V_c - V_g)/d$ $(I_c/A)^{\gamma}$.

We see that the correct order of magnitude is achieved in all the cases.

Finally, we compare our grid model with that of K. J. Mclean et al. These authors take an array of parallel wires, like that of Fig. 6, assume weak electrical interaction among the wires and apply ideas akin to the grid theory. In most of their measurements the electric field in the grid-plate space was higher than the field above the grid. On the other hand, the theory presented here applies in the opposite case, since only in this condition may a "recombination" take place. Although oversimplified, our model correctly predicts higher electrical transparency for higher optical transparency (intuitively smaller γ). Preliminary tests carried out with planar grids confirm the presence of the two regimes, that is, the space charge and the γ power law for constant corona current. According to the theory of Sec. III, we should expect to fit the measured characteristics with the single parameter γ , since q would be approximately a constant. However, this is not so and we have attributed this to the lack of uniformity in the current distribution (Warburg law 8). With our double grid this effect was minimized.

ACKNOWLEDGMENTS

The authors are greatly indebted to Professor J. A. Giacometti for his assistance in the experiment. They also express their gratitude to FAPESP and TELEBRAS for the concession of research grants.

- ¹B. Gross, J. A. Giacometti, G. F. Leal Ferreira, and O. N. Oliveira Jr.,
- J. Appl. Phys. 56, 1487 (1984).
- ²J. A. Giacometti, Ph.D. thesis, IFQSC, USP, 1982.
- ³A. Goldman, R. Haug, and R. V. Latham, J. Appl. Phys. 47, 2418 (1976).
- ⁴R. A. Moreno, Ph.D. thesis, IFQSC, USP, 1977.
- ⁵E. Weber, Electromagnetic Theory (Dover, New York, 1965), p. 291.
- ⁶R. C. Hughes, J. Appl. Phys. 51, 5933 (1981).
- ⁷K. J. Mclean, Z. Herceg, and R. I. Boccola, J. Electrostatics 9, 211 (1981).
- ⁸R. S. Sigmond, J. Appl. Phys. 53, 891 (1982).
- ⁹L. B. Loeb, *Electrical Coronas* (University of California, Berkeley, 1965), p. 405.
- ¹⁰R. Langevin, Ann. Chim. Phys. 28, 287 (1903).